ELSEVIER

Cooling of a two-dimensional space with one or more streams making one or more passes

D. Homentcovschi
Institute of Applied Mathematics, Bucharest, Romania
G. Stanescu
Department of Mathematics, University of Rio Grande, Rio Grande RS, Brazil
A. Bejan
Department of Mechanical Engineering and Materials Science, Duke University, Durham, NC, USA

This is a study of a fundamental problem in electronic cooling; namely, conduction in a two-dimensional (2-D) domain cooled by one or more streams that make one or more passes. The fundamental objective is to determine the relation between the chosen cooling patterns and the temperature distribution in the domain, with particular emphasis on the maximum and minimum temperatures. The practical objective is to develop a consistent method of evaluating the cooling performance of various flow patterns, so that the trends of performance improvement are visible, and the selection of the best cooling pattern can be made with minimum additional computation. The method begins with a general analytical treatment based on the use of finite cosine Fourier transforms, and ends with an efficient numerical implementation of the analytical formulation. The results show that cooling patterns with more cold inlets maintain lower hot-spot temperatures. Furthermore, patterns where adjacent flow passes are oriented in counterflow guarantee more uniform temperature distributions than patterns with adjacent passes in parallel flow. The distribution of temperature is also illustrated experimentally for 15 cases using three different flow patterns.

Keywords: forced convection; electronic cooling; flow pattern selection

Introduction

In this paper we consider a basic heat transfer problem that finds application in the cooling of electronics. It is the problem of cooling a conducting body by placing it in convective contact with one or more streams. Critical is the relation between the streams (their flow pattern), the maximum temperature, and the uniformity of the temperature distribution in the conducting body (Moffat and Ortega 1988; Peterson and Ortega 1990).

For example, in a printed circuit board or in all the components mounted on the floor of the interior of a personal computer, the heat is generated internally. It is conducted through the solid parts and is removed by air that blows over the hot surfaces. A modern trend is to use multiple streams (e.g., channels, jets) directed especially at those areas that tend to develop hot spots (Hingorani et al. 1994; Lall et al. 1994; Sugavanam et al. 1994; Kamath 1994; Creel and Nelson 1994).

Address reprint requests to Prof. A. Bejan, Mechanical Engineering and Materials Science, Duke University, Durham, NC 27708-0300, USA.

Received 21 October 1994; accepted 2 October 1995

We examine this problem by focusing on the two-dimensional (2-D) model shown in Figure 1a. The conducting body is rectangular with dimensions $L_x \times L_y$ and generates heat locally at the rate q'''. We assume that q''' is distributed uniformly, however, the analytical and numerical treatment presented in the Mathematical formulation and Numerical method sections can be used for a general distribution $q'''(x, y)$. The body temperature $T(x, y)$ is the chief unknown.

The body is cooled by one or more streams of mass flow rate $\dot{m}$, which are aligned with L_y. Two streams with two passes each are illustrated in Figure 1a. The streams flow over the $L_x \times L_y$ surface, or through channels machined into the body. Each stream is characterized by a bulk temperature T_c that varies along the path traveled by the stream. The stream cross section is characterized by a wetted perimeter p, and a constant heat transfer coefficient h between the solid and the coolant. Parameters $\dot{m}$, p, and h are assumed known.

The objectives are to devise an effective method for evaluating the relative performance of various cooling patterns, to uncover general trends of performance improvement, and to select the best cooling pattern within minimum additional computation. The approach we have chosen is a combination of analysis and numerical work. We develop the analytical part as far as possible in order to visualize the inner parts of the conjugate heat

Int. J. Heat and Fluid Flow 17: 78–88, 1996
© 1996 by Elsevier Science Inc.
655 Avenue of the Americas, New York, NY 10010

0142-727X/96/$15.00
SSDI 0142-727X(95)00086-0

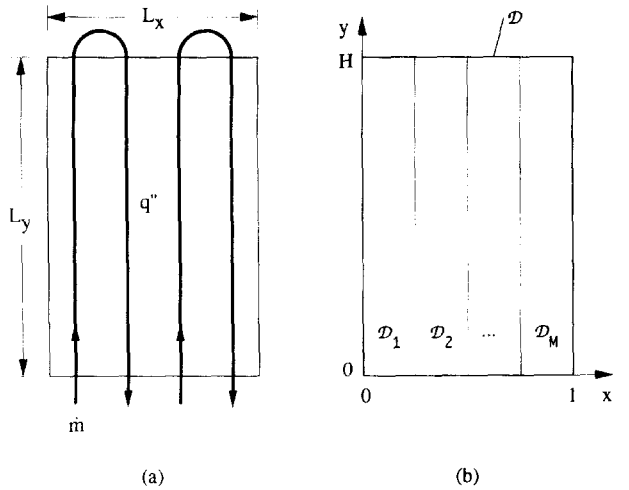

Figure 1 (a) Two-dimensional (2-D) body with internal heat generation and cooling provided by several streams with several passes each; (b) dimensionless representation of the conducting domain

transfer process and to minimize the required computational work.

Mathematical formulation

Problem statement. Consider the (2-D) conducting domain (the "plate") $\mathscr{D}$ shown in Figure 1b, where the length of the domain in the x direction is used as reference length. The domain is divided into M parallel strips ($\mathscr{D}_1, \mathscr{D}_2, \ldots, \mathscr{D}_M$), which are described by the dimensionless abscissa values $0 = x_0 < x_1 < x_2 < \ldots < x_{M-1} < x_M = 1$. Note also that $H = L_y/L_x$.

We begin with the analysis of a domain cooled by a single stream, with a single inlet and a single outlet. In Figure 1b, for example, the stream travels strips $\mathscr{D}_1, \mathscr{D}_3, \ldots$ in the positive y direction and returns along strips $\mathscr{D}_2, \mathscr{D}_4, \ldots$ flowing in the negative y direction. More complicated flow patterns can be analyzed similarly and are described in the body of the paper.

The mathematical problem consists of determining the plate temperature $\theta(x, y)$ and the coolant bulk temperature $\theta_c^{(m)}(y)$ along the mth strip, so that

$$\frac{\partial^2\theta}{\partial x^2} + \frac{\partial^2\theta}{\partial y^2} - \mathrm{Bi}\left[\theta - \theta_c^{(m)}(y)\right] + 1 = 0 \tag{1}$$

$$\frac{\mathrm{d}\theta_c^{(m)}}{\mathrm{d}\sigma} + k_m\left[\theta_c^{(m)}(y) - \hat{\theta}^{(m)}(y)\right] = 0 \tag{2}$$

Equation 1 is for steady heat conduction in $\mathscr{D}$, with convection to a fluid that flows through the domain (or sweeps the surface shown in Figure 1), and with uniform internal heat generation. Equation 2 accounts for the temperature increase experienced by the stream as it travels along the curvilinear path of coordinate σ (note: $\sigma = y$ in $\mathscr{D}_1$, $\sigma = 2H - y$ in $\mathscr{D}_2$, $\sigma = 2H + y$ in $\mathscr{D}_3$, etc.). We also used $k_m = \mathrm{d}_m$ NTU, $d_m = x_m - x_{m-1}$, and

$$\hat{\theta}^{(m)}(y) = \frac{1}{\mathrm{d}_m}\int_{x_{m-1}}^{x_m} \theta(x, y)\,\mathrm{d}x \tag{3}$$

where $\hat{\theta}^{(m)}(y)$ is the plate temperature averaged over the width of the mth strip. The dimensionless groups Bi and NTU are defined in the Notation.

The function $\theta(x, y)$ must have first-order continuous derivatives inside $\mathscr{D}$ and must satisfy the following boundary condition:

$$\left.\frac{\partial\theta}{\partial n}\right|_{\mathscr{B}} = 0 \tag{4}$$

Notation

$\mathscr{B}$	boundary of domain $\mathscr{D}$
Bi	Biot number, hL_x^2/kt
c_p	coolant specific heat at constant pressure, kJ/kg · K
d_m	dimensionless width of the strip, $x_m - x_{m-1}$
D_h	hydraulic diameter, m
$\mathscr{D}$	two-dimensional conducting domain
$\mathscr{D}_m$	subdomain of the mth strip
$\mathscr{F}_c$	finite cosine Fourier transform
h	heat transfer coefficient between plate and coolant averaged over p, W/m^2 K
H	dimensionless height of the plate, L_y/L_x
k	plate thermal conductivity, W/m · K
k_m	dimensionless group, d_m NTU
L_x	plate length, m
L_y	plate height, m
$\dot{m}$	stream mass flow rate, kg/s
M	total number of strips
NTU	number of heat transfer units, $hL_x^2/\dot{m}c_p$
p	wetted perimeter of the stream cross section, m
q''	heat generation rate per unit of plate area, W/m^2
Re_{in}	air inlet Reynolds number
s	coordinate along the stream, m
t	plate thickness, m
T	plate temperature, K
T_c	coolant bulk temperature, K
T_0	coolant inlet temperature, K
U	air mean velocity
(x, y)	dimensionless coordinates, $(x^*/L_x, y^*/L_x)$
x^*, y^*	physical coordinates, m

Greek

θ	dimensionless plate temperature, $(T - T_0)/(q''L_x^2/kt)$
θ_c	dimensionless coolant temperature, $(T_c - T_0)/(q''L_x^2/kt)$
$\hat{\theta}^{(m)}(y)$	dimensionless average temperature along the mth strip
ν	kinematic viscosity
σ	dimensionless coordinate along the stream, s/L_x

Subscripts

f	final (outlet)
j	jth iteration
max	maximum
min	minimum
n	nth spectral component
0	initial (inlet)

Superscript

m	mth strip

Here n is the external normal to the boundary $\mathscr{B}$ of the plate domain $\mathscr{D}$. Note that Equation 4 does not refer to the boundary of one of the subdomains (strips) $\mathscr{D}_m$: the boundary conditions between adjacent strips are given in Equations 12 and 13. The coolant temperature satisfies the inlet condition

$$\theta_c^{(1)}(0) = 0 \tag{5}$$

and the continuity conditions

$$\theta_c^{(1)}(H) = \theta_c^{(2)}(H)$$

$$\theta_c^{(2)}(0) = \theta_c^{(3)}(0) \ldots \tag{6}$$

It can be shown that the problem consisting of Equations 1 and 2 and conditions 4–7 has, at most, one solution. The proof of this uniqueness theorem is omitted for brevity.

Spectral representation of the plate temperature

We assume for the time being that the coolant temperature function $\theta_c^{(m)}(y)$ is known. Equation 1 can be rewritten as follows:

$$\frac{\partial^2\theta^{(m)}}{\partial x^2} + \frac{\partial^2\theta^{(m)}}{\partial y^2} - \mathrm{Bi}\theta^{(m)} = -1 - \mathrm{Bi}\theta_c^{(m)}(y) \tag{7}$$

where the superscript of $\theta^{(m)}$ means that we are focusing on the plate temperature distribution $\theta(x, y)$ in the subdomain $\mathscr{D}_m$.

Next, we introduce the finite cosine Fourier transform $\mathscr{F}_c$ of the function $\theta^{(m)}(x, y)$ with respect to y:

$$\theta^{(m)}(x, y) = {\sum_{n=0}^{\infty}}' a_n^{(m)}(x)\cos\left(\frac{n\pi}{H}y\right) = \mathscr{F}_c^{-1}\left[a_n^{(m)}(x)\right] \tag{8}$$

$$a_n^{(m)}(x) = \frac{2}{H}\int_0^H \theta^{(m)}(x, y)\cos\left(\frac{n\pi}{H}y\right)\mathrm{d}y = \mathscr{F}_c\left[\theta^{(m)}(x, y)\right] \tag{9}$$

The prime on Σ in Equation 8 is a reminder that in that summation, the first term must be multiplied by $1/2$. From Equation 8,

$$\frac{\partial}{\partial y}\theta^{(m)}(x, y) = -\sum_{n=1}^{\infty} a_n^{(m)}(x)\frac{n\pi}{H}\sin\left(\frac{n\pi}{H}y\right) \tag{10}$$

therefore

$$\left.\frac{\partial\theta^{(m)}}{\partial y}\right|_{(x,0)} = \left.\frac{\partial\theta^{(m)}}{\partial y}\right|_{(x,H)} = 0 \tag{11}$$

which means that the boundary condition on the $y = 0$ and $y = H$ sides of the $\mathscr{D}$ rectangle are satisfied. In the case of constant-temperature boundary conditions, a finite sine Fourier transform can be used, and the analysis follows the same main steps.

Because $\theta(x, y)$ must have first-order continuous partial derivatives inside $\mathscr{D}$, we must impose the following conditions:

$$\theta^{(m)}(x_m, y) = \theta^{(m+1)}(x_m, y) \tag{12}$$

$$\left.\frac{\partial\theta^{(m)}}{\partial x}\right|_{(x_m,y)} = \left.\frac{\partial\theta^{(m+1)}}{\partial x}\right|_{(x_{m+1},y)}, \qquad (m = 1, \ldots, M-1) \tag{13}$$

Furthermore, boundary condition 4 requires the following conditions on the $x = 0$ and $x = 1$ sides of the overall domain:

$$\left.\frac{\partial\theta^{(1)}}{\partial x}\right|_{(0,y)} = \left.\frac{\partial\theta^{(M)}}{\partial x}\right|_{(1,y)} = 0 \tag{14}$$

Applying the $\mathscr{F}_c$ transform to formulas 12–14, we obtain the corresponding relations in the spectral domain:

$$a_n^{(m)}(x_m) = a_n^{(m+1)}(x_m) \tag{15}$$

$$\left.\frac{\mathrm{d}}{\mathrm{d}x}a_n^{(m)}\right|_{(x_m)} = \left.\frac{\mathrm{d}a_n^{(m+1)}}{\mathrm{d}x}\right|_{(x_m)}, \qquad (n = 1 \ldots M-1) \tag{16}$$

$$\left.\frac{\mathrm{d}a_n^{(1)}}{\mathrm{d}x}\right|_{(0)} = \left.\frac{\mathrm{d}a_n^{(M)}}{\mathrm{d}x}\right|_{(1)} = 0 \tag{17}$$

The $\mathscr{F}_c$ transform of Equation 7 yields

$$\frac{\mathrm{d}^2a_n^{(m)}}{\mathrm{d}x^2} - \left[\mathrm{Bi} + \left(\frac{n\pi}{H}\right)^2\right]a_n^{(m)} = -2\delta_{n0} - \mathrm{Bi}\theta_{cn}^{(m)} \tag{18}$$

where

$$\theta_c^{(m)}(y) = {\sum_{n=0}^{\infty}}' \theta_{cn}^{(m)}\cos\frac{n\pi}{H}y \tag{19}$$

Here δ_{nm} is 1 when $n = m$, and 0 otherwise. In conclusion, in the spectral domain the partial differential Equation 7 is replaced by the ordinary differential Equation 18, which has the general solution

$$a_n^{(m)}(x) = \frac{2}{\mathrm{Bi}}\delta_{n0} + \frac{\mathrm{Bi}}{r_n^2}\theta_{cn}^{(m)} + \frac{\mathrm{Bi}}{r_n^2}\left[A_n^{(m)}\cosh(r_n x) + B_n^{(m)}\sinh(r_n x)\right] \tag{20}$$

where $r_n = [\mathrm{Bi} + (n\pi/H)^2]^{1/2}$. The constants $A_n^{(m)}$ and $B_n^{(m)}$ are obtained from conditions 15–17; after considerable algebra, we obtain

$$A_n^{(m)}\cosh(r_n x) + B_n^{(m)}\sinh(r_n x) = \sum_{m'=m}^{M-1}\frac{\cosh(r_n x)\cdot\sinh\left[r_n(1-x_{m'})\right]}{\sinh(r_n)}\left[\theta_{cn}^{(m'+1)} - \theta_{cn}^{(m')}\right] - \sum_{m'=1}^{m-1}\frac{\sinh(r_n x_{m'})\cdot\cosh\left[r_n(1-x)\right]}{\sinh(r_n)}\left[\theta_{cn}^{(m'+1)} - \theta_{cn}^{(m')}\right] \tag{21}$$

where $x \in [x_{m-1}, x_m]$; $m = 1, \ldots, M$.

It is worth noting that in the case of a nonuniform distribution of heat generation, the heat source intensity will replace $\delta_{n,0}$ in Equation 18. Likewise, if the plate is anisotropic, we must distinguish between the directional thermal conductivities k_x and k_y: in this case the expression in the square brackets in Equation 18 is replaced by $[\mathrm{Bi} + (n\pi/H)^2 k_y/k_x]$. Nonuniformities in the end-turn regions can also be taken into account in the fully numerical method (Fully numerical method section) by including the variation of the heat transfer coefficient with the s coordinate along the strip.

Equations 8, 20, and 21 constitute the spectral representation of the temperature distribution over the plate. This representation contains the unknown spectral components of the coolant temperature, $\theta_{cn}^{(m)}$.

Spectral representation of the coolant temperature

We begin with the observation that the differential Equation 2 for the coolant temperature contains the unknown function $\hat{\theta}^{(m)}(y)$. To obtain a second relation between $\theta_c^{(m)}$ and $\hat{\theta}^{(m)}$ we average

Equation 1 with respect to x, across the strip $\mathscr{D}_m$, and the result is

$$\frac{d^2\hat{\theta}^{(m)}(y)}{dy^2} - Bi\hat{\theta}^{(m)}(y) + Bi\theta_c^{(m)}(y) = -1 - \frac{1}{d_m}\left[\frac{\partial\theta^{(m)}}{\partial x}(x_m, y) - \frac{\partial\theta^{(m)}}{\partial x}(x_{m-1}, y)\right] \quad (22)$$

The boundary conditions for $\hat{\theta}^{(m)}(y)$ of Equation 22 are obtained by writing Equation 4 along the top and bottom edges of the plate (Figure 1), and then averaging the equations over the width of the strip:

$$\left.\frac{d\hat{\theta}^{(m)}}{dy}\right|_{(y=0)} = \left.\frac{d\hat{\theta}^{(m)}}{dy}\right|_{(y=H)} = 0 \quad (23)$$

To determine the coolant temperature we must integrate Equations 2 and 22 subject to the initial and boundary conditions 5, 6, and 23. This system is not closed, because of the term containing the derivative of $\theta^{(m)}(x, y)$ in Equation 22. To close the system, we make an additional simplification that begins with the observation that the first term on the right side of Equation 22 represents the intensity of the heat source in the plate. Then we can regard the second term as a source term, and write $\alpha =$ constant for the sum of the two source terms; i.e., for the entire right side of Equation 22. Equations 2 and 22 become

$$\pm\frac{d\theta_c^{(m)}}{dy} + k_m\left[\theta_c^{(m)}(y) - \hat{\theta}^{(m)}(y)\right] = 0 \quad (24)$$

$$\frac{d^2\hat{\theta}^{(m)}}{dy^2} + Bi\theta_c^{(m)}(y) - Bi\hat{\theta}^{(m)}(y) = \alpha, \qquad (m = 1, \ldots, M) \quad (25)$$

In Equation 24, the + sign is for odd strips, and the − sign for even strips. The equation for even strips can be obtained from the equation for odd strips by replacing k_m with $-k_m$; therefore, we show only the solutions for odd strips.

We solved the system 24 and 25 by using Laplace transforms. In the interest of brevity, we omit the analysis and list only the final expressions:

$$\theta_c^{(m)}(y) = \theta_{c0}^{(m)} + c_0 S^{(m)}(y) + \alpha\left[\frac{k_m^2}{Bi^2}C^{(m)}(y) - \frac{k_m^2}{Bi^2} - \alpha\frac{k_m}{Bi}y\right] \quad (26)$$

$$\hat{\theta}^{(m)}(y) = \theta_{c0}^{(m)} - \frac{\alpha}{Bi}\left(1 - k_m y - \frac{k_m^2}{Bi}\right) + \left(c_0 + \alpha\frac{k_m^2}{2Bi^2}\right)C^{(m)}(y) + \frac{1}{2}\left(c_0 + \frac{2}{Bi}\alpha + \alpha\frac{k_m^2}{2Bi^2}\right)S^{(m)}(y) \quad (27)$$

where

$$C^{(m)}(y) = \exp(-k_m y/2)\cdot\cosh(\Delta_m y) \quad (28)$$

$$S^{(m)}(y) = k_m\cdot\exp(-k_m y/2)\cdot\sinh(\Delta_m y)/\Delta_m \quad (29)$$

and $\Delta_m = (Bi + k_m^2/4)^{1/2}$. Solutions 26 and 27 satisfy the initial and boundary conditions with the exception of the second of Equations 23: this equation is used to determine the constant c_0.

The spectral components of the coolant temperature can be obtained also analytically by means of the relations:

$$\mathscr{F}_c\left\{\begin{matrix} e^{-\beta y} & \begin{matrix}\cosh\\ \sinh\end{matrix} & (\Delta y)\end{matrix}\right\} = \frac{1}{H}\left\{(\beta - \Delta)\frac{1 - (-1)^n e^{-(\beta-\Delta)H}}{(\beta-\Delta)^2 + n^2\pi^2/H^2} \pm (\beta + \Delta)\frac{1 - (-1)^n e^{-(\beta+\Delta)H}}{(\beta+\Delta)^2 + n^2\pi^2/H^2}\right\} \quad (30)$$

Numerical method

In the preceding section, we formulated the mathematical problem in two parts. One part concerns the plate temperature, which is obtained based on Equations 8, 20, and 21. The other part deals with the coolant bulk temperature and is described by Equations 2 and 22. The two parts are coupled, as the plate temperature enters Equation 22 through its x-derivative along the boundary between adjacent strips. The numerical development of the solution consists of iterating between the two parts of the problem.

We developed two numerical methods for determining the coolant temperature. The first method (Combined analytical and numerical method section) is simpler and faster, and is based on treating the second term on the right side of Equation 22 as a supplementary source term, by means of the $\alpha =$ constant approximation. This approach enables us to determine analytically the coolant temperature and its spectral components. The analytical method works only in cases where the strips are not very narrow. The second method (Fully numerical section) consists of integrating numerically the system of Equations 2 and 22 subject to the specified initial and boundary conditions and is based on determining numerically the spectral components of $\theta_c(y)$.

Combined analytical and numerical method

The numerical algorithm consists of the following steps:

(1) The initial solution is determined by assuming $\alpha = -1$ (i.e., no additional sources along each strip) and *M independent* strips; i.e., zero coolant temperature at the entrance to each strip. The coolant temperature at the outlet of each strip $\theta_{cf,0}^{(m)}$ is obtained by using Equation 26: in this way it becomes possible to determine the first approximation of the coolant temperatures at the strip inlets. For example, if there are only four strips and a single stream, we have

$$\theta_{c0}^{(1)} = 0$$
$$\theta_{c0,0}^{(2)} = \theta_{cf,0}^{(1)}$$
$$\theta_{c0,0}^{(3)} = \theta_{cf,0}^{(1)} + \theta_{cf,0}^{(2)}$$
$$\theta_{c0,0}^{(4)} = \theta_{cf,0}^{(1)} + \theta_{cf,0}^{(2)} + \theta_{cf,0}^{(3)} \quad (31)$$

(2) Equation 26 with $\alpha = -1$ provides the first approximation for the coolant temperature. Equation 30 yields the corresponding spectral components and new approximations for the coolant temperature at the strip outlets $\theta_{cf,1}^{(m)}$.

(3) Equations 8, 20, and 21 yield the approximations for the plate temperature, $\theta_j^{(m)}(x, y)$, $j = 1, \ldots$

(4) An approximation for the source term $\alpha_j^{(m)}$, is obtained by using the expression on the right side of Equation 22. New

approximations for the coolant inlet temperatures are obtained next:

$$\bar{\theta}^{(1)}_{c0,j} = 0$$

$$\bar{\theta}^{(m)}_{c0,j} = \theta^{(m-1)}_{cf,j}, \qquad (m = 2, \ldots, M) \tag{32}$$

(5) Relaxed iterations are performed for the source terms and the inlet temperatures,

$$\alpha^{(m)}_j = (1-\lambda)\alpha^{(m)}_{j-1} + \lambda\bar{\alpha}^{(m)}_j$$

$$\theta^{(m)}_{c0,j} = (1-\lambda)\theta^{(m)}_{c0,j-1} + \lambda\bar{\theta}^{(m)}_{c0,j} \tag{33}$$

where $m = 1, \ldots, M$; $j = 1, \ldots,$ and λ is a relaxation parameter less than 1. New approximations for the coolant temperature $\theta^{(m)}_{c,j}(y)$ and strip outlet temperature $\theta^{(m)}_{cf,j}$ are obtained from Equation 26.

(6) Steps (3–5) are repeated until the first three significant digits of $\alpha^{(m)}_j$ and $\theta^{(m)}_{c0,j}$ do not change anymore.

Fully numerical method

According to the second approach, the coolant temperature along each strip is obtained by solving numerically the system 2 and 22, with the boundary conditions 23 and the initial conditions resulting from Equations 5 and 7. Noting that Equation 19 for the plate temperature contains the spectral components of the coolant temperature, we calculated the coolant temperature in a grid of 16–32 equidistant points across each strip. The system of differential equations to be solved is linear, therefore we solved the boundary value problem 23 by means of two initial value problems with the initial data

$$\hat{\theta}^{(m)}_I(0) = 0\,; \qquad \left.\frac{d\hat{\theta}^{(m)}_I}{dy}\right|_{(0)} = 0\,; \qquad \theta^{(m)}_{cI}(0) = \theta^{(m)}_{c0} \tag{34}$$

$$\hat{\theta}^{(m)}_{II}(0) = \gamma\,; \qquad \left.\frac{d\hat{\theta}^{(m)}_{II}}{dy}\right|_{(0)} = 0\,; \qquad \hat{\theta}^{(m)}_{cII}(0) = 0 \tag{35}$$

The constant γ is determined so that

$$\left.\frac{d\hat{\theta}^{(m)}}{dy}\right|_{(H)} = \left.\frac{d\hat{\theta}^{(m)}_I}{dy}\right|_{(H)} + \gamma\left.\frac{d\hat{\theta}^{(m)}_{II}}{dy}\right|_{(H)} = 0 \tag{36}$$

The second method is expected to be more accurate than the first method when the strips are not very narrow; i.e., when the coolant makes very few passes over the conducting domain. Accuracy tests and the relative performance of the two methods are documented at the end of the next section.

Numerical results for configurations with four strips

We illustrate the methodology developed in the Mathematical formulation and Numerical method sections by showing the results obtained for four flow patterns, which are labeled A, B, C, and D in the insets of Figures 2–5. In each case, the conducting domain is square ($H = 1$) and is divided into four strips. The cooling patterns differ with respect to the number of streams used (i.e., the number of T_0-cold inlets), the number of passes executed by each stream, and the relative direction of two adjacent streams. For each pattern, we solved the problem for Bi = 0.1, 1, 10, and 50, and for a sufficient number of NTU values in the range 0.1–10 so that the curves plotted in Figures 2–5 are smooth. The isotherm patterns exhibited in each of Figures 2–5 correspond to NTU = 1 and Bi = 1.

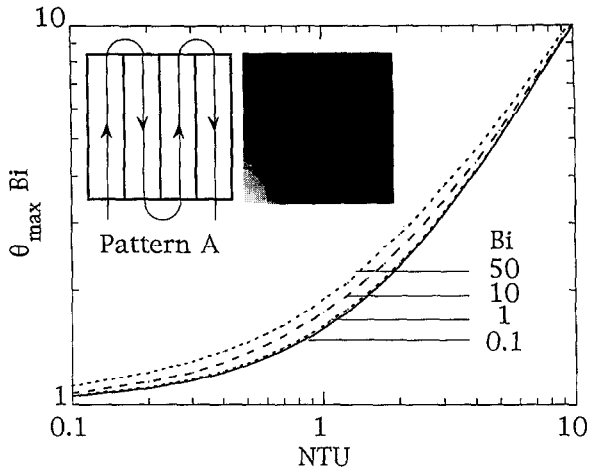

Figure 2 Maximum temperature and temperature field for cooling pattern A: one stream, four passes ($H = 1$)

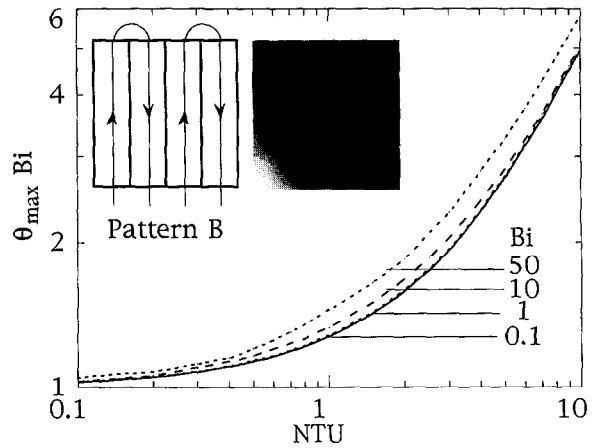

Figure 3 Maximum temperature and temperature field for cooling pattern B: two streams, two passes each ($H = 1$)

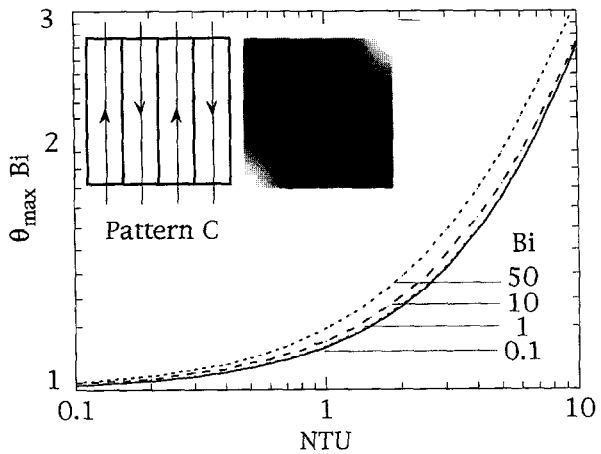

Figure 4 Maximum temperature and temperature field for cooling pattern C: four counterflow streams, one pass each ($H = 1$)

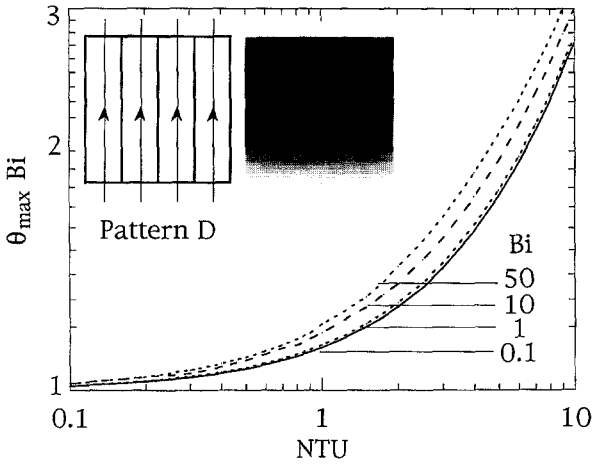

Figure 5 Maximum temperature and temperature field for cooling pattern D: four parallel-flow streams, one pass each ($H = 1$)

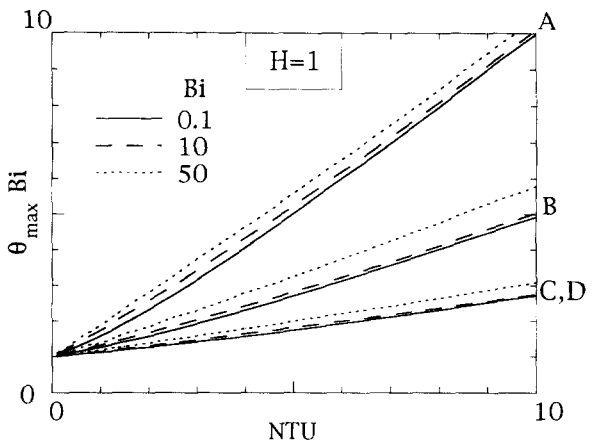

Figure 6 Linear-graph summary of the maximum temperature results of Figures 2–5

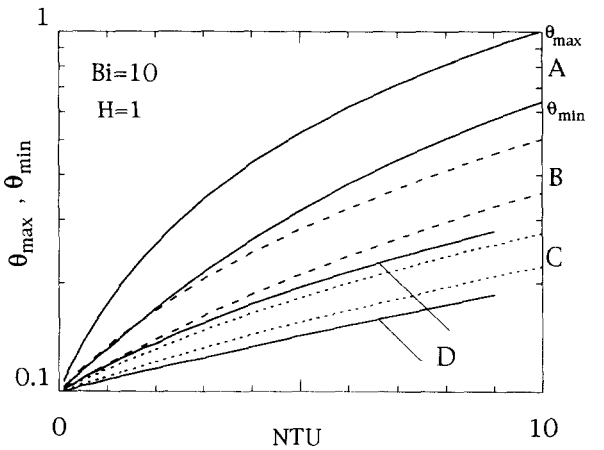

Figure 7 Comparison between the maximum and minimum body temperatures when $H = 1$ and Bi = 10

A first conclusion, is that from the point of view of the value and behavior of the maximum temperature

$$\theta_{max} = \frac{T_{max} - T_0}{q'' L_x^2 / kt} \tag{37}$$

two of the cooling patterns, C and D, are essentially equivalent (compare Figures 4 and 5). One important difference is that, in the case of pattern C, the θ_{max} value occurs in the two "exit" corners; whereas, in pattern D, the maximum temperature is pushed to the top boundary ($y = H$): these features are illustrated by the isotherm patterns shown as insets in Figures 4 and 5, where dark represents hot, and light represents cold.

Another interesting aspect of the results shown in Figures 2–5 is that the curves drawn for each cooling pattern fall almost on top of one another: this is because we have used the group θ_{max}Bi on the ordinate. The linear-graph summary shown in Figure 6 suggests that when NTU exceeds approximately 5, the group θ_{max}Bi increases almost linearly with the NTU. For $H = 1$, this linear expression is

$$\theta_{max} = \alpha_j + \beta_j \frac{\text{NTU}}{\text{Bi}} \tag{38}$$

where $(\ )_j$ indicates the pattern (A, B, C, or D), and α_j and β_j are the empirical coefficients listed in Table 1. Worth noting is that α_j depends on the flow pattern and Bi; whereas, β_j depends only on the flow pattern.

In Figure 7 we see the two curves drawn for each flow pattern at fixed H and Bi: the upper curve is for the hot-spot temperature θ_{max}, while the lower curve represents the minimum temperature θ_{min} in the two-dimensional conducting domain. Both temperatures drop as the flow pattern changes form A to B, and finally to C or D. The C pattern is attractive not only because θ_{max} is the lowest, but also because the difference $\theta_{max} - \theta_{min}$ is the smallest (i.e., the temperature field in the conducting domain is the most uniform). In Figure 7 the Biot number was set at 10. The general outlook of the figure does not change as Bi decreases, except that the difference $\theta_{max} - \theta_{min}$ becomes smaller. The θ_{max} and θ_{min} curves are indistinguishable when Bi is smaller than approximately 1.

The effect of the shape of the conducting domain is documented by Figure 8a and b. The group θ_{max}Bi/H used on the ordinate shows that in the large NTU limit the maximum temperature is proportional to H. In the small NTU limit θ_{max} is independent of H and cooling pattern. Once again, we note the linear dependence between θ_{max} and NTU in the large NTU limit, in accordance with Figure 6. Figure 8a, b also shows the additional effect of the Biot number, that is beyond the role played by Bi in the ordinate group θ_{max}Bi/H. This effect is felt when Bi is greater than approximately 10.

We performed several tests to determine the accuracy and speed of the numerical method used. To see the effect of the number of terms retained in the finite cosine Fourier transformation, we ran the same case twice, by using 16 and 32 terms. The

Table 1 Numerical coefficients for the linear σ_{max} correlation 38 ($H = 1$, NTU ≥ 5)

Flow pattern (j)	α_j				β_j
	Bi = 0.1	1	10	50	
A	1.5	0.17	0.03	0.013	0.98
B	3.5	0.39	0.044	0.020	0.45
C,D	7.2	0.72	0.077	0.020	0.20

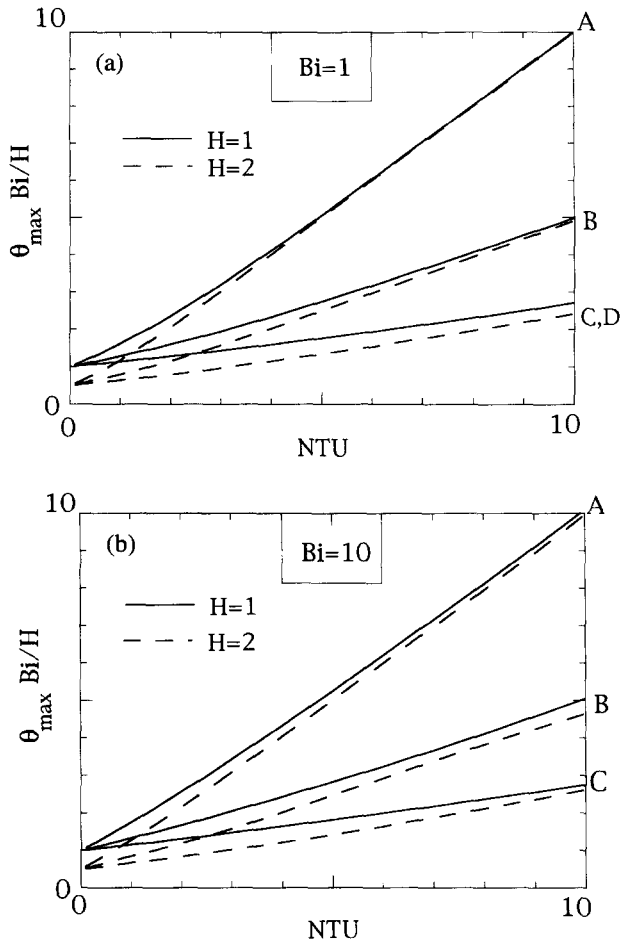

Figure 8 The effect of the conducting domain shape (H) on the maximum temperature

relative difference between the θ_{max} values produced by the two runs was less than 10^{-3}.

The two numerical methods described in the Combined analytical and numerical method and the Fully numerical method sections were compared for $H = 1$, Bi = 1 and $0.1 \leq$ NTU ≤ 10. Plotted in Figure 9 is the relative difference between the hot-spot temperatures calculated with the two methods, $(\theta_{max,1} - \theta_{max,2})/\theta_{max,2}$, where subscripts 1 and 2 refer, respectively, to the analytical-numerical method and the fully numerical method. The figure shows that when $H = 1$, the two methods agree within two significant digits. We repeated this test for $H = 2$ and found that the disagreement between the two methods is significant at relatively large NTU values. When the $\mathscr{D}_1, \ldots \mathscr{D}_4$ strips are narrow the model used to develop the analytical-numerical method breaks down.

The method used in the paper to determine the plate temperature is in fact a Fast Solver for the special problem we have formulated. This method is superior to any other fully numerical scheme such as the finite-differences or finite-elements methods used for determining the solution to the two-dimensional partial differential equation.

The results presented in this section for $H = 1$ were obtained using the simpler, analytical-numerical method. The $H = 2$ cases were computed using the fully numerical method. Figure 10 shows a comparison of the computation times required by the two methods. When it is suitable (appropriate), the analytical-numerical method is at least ten times faster than the fully numerical method.

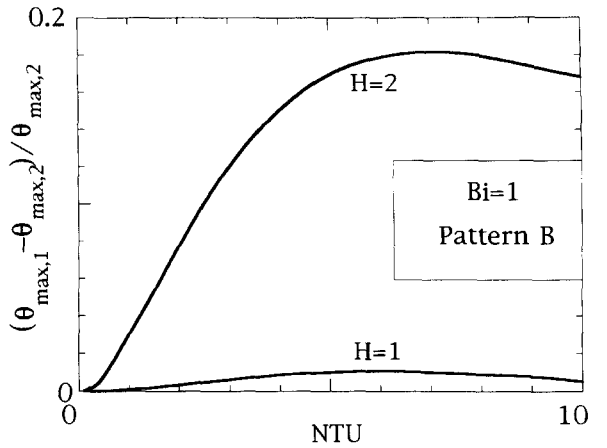

Figure 9 The relative difference between the maximum temperatures calculated using the numerical methods described in the analytical-numerical section and the fully numerical section

The iteration between the two parts of the mathematical formulation (the Spectral representation sections) was terminated when the calculated coolant temperature became constant to the first three significant digits. The maximum number of iterations was 200, however, in most of the runs that number was less than 50. The computation time was reduced considerably by using fast Fourier transformation algorithms for summing Fourier series and calculating Fourier coefficients.

Numerical results for other configurations

In this section, we illustrate the versatility of the method by considering configurations with two or three strips, and uniform or nonuniform heat generation. The results are summarized in Figures 11–13, which show only the flow patterns, the maximum and minimum temperatures, and the actual locations of θ_{max} and θ_{min}.

Figure 11 shows the results for the three cooling patterns that can be used when the conducting domain is relatively long in the direction of flow. The hot-spot temperature decreases when the number of streams (or cold inlets) increases. Furthermore, counterflow provides better temperature uniformity than parallel flow; i.e., a small difference between θ_{max} and θ_{min}. In Figure 11, the

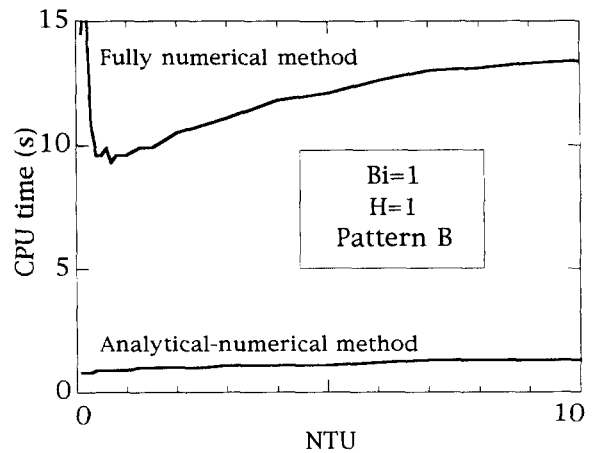

Figure 10 Comparison between the computation times required by the two numerical methods used

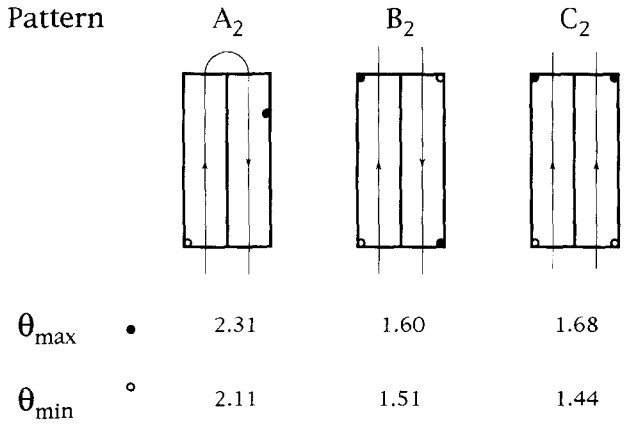

Figure 11 Performance of cooling patterns with two strips when Bi = 1, NTU = 1, and $H = 2$

best performance belongs to pattern B_2. Worth noting is that the B_2 pattern has been used as a laboratory technique for maintaining a wall at nearly uniform temperature (Deaver and Eckert 1970; Beloff et al. 1988).

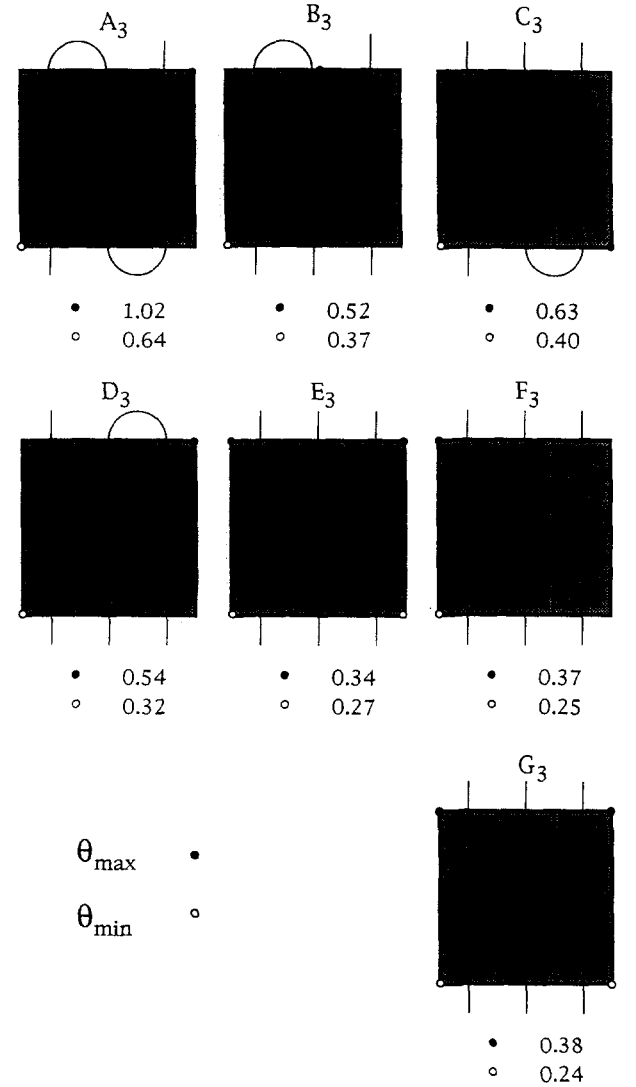

Figure 12 Performance of cooling patterns with three strips and uniform heat generation when Bi = 10, NTU = 10, and $H = 1$

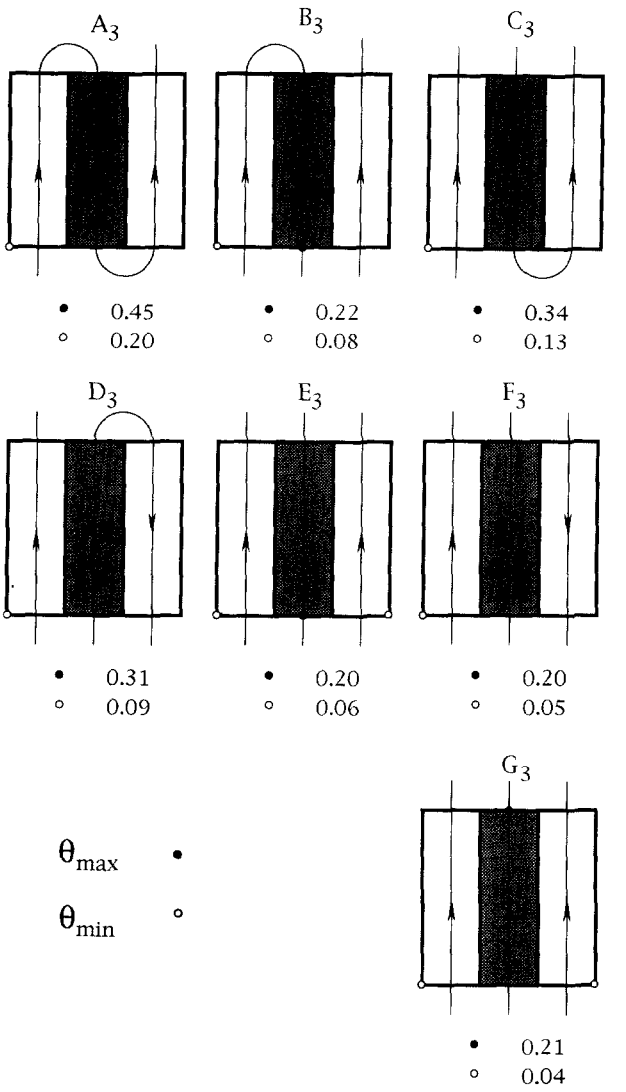

Figure 13 Performance of cooling patterns with three strips and nonuniform (central strip) heat generation when Bi = 10, NTU = 10, and $H = 1$

The performance of cooling patterns for square conducting domains with three strips is documented in Figure 12. Once again, all the temperatures decrease as the number of cold inlets increases from one cold inlet in configuration A_3 to three cold inlets in configurations $E_3 - G_3$. The configuration with the lowest hot-spot temperature and the smallest difference between θ_{max} and θ_{min} is the counterflow of three streams with three cold inlets (E_3).

The numerical method developed in this study can be further applied to conducting domains with nonuniform distributions of heat generation. In general, the heat generation can be distributed in any number of isolated ractangular or square patches inside the $L_x \times L_y$ domain. A first step in this direction is illustrated in Figure 13, which shows a domain with a central strip with heat generation and two lateral strips that act as heat spreaders (Hingorani et al. 1994). The performance of the seven cooling patterns can be compared with the corresponding results for the case when the entire domain generates heat (Figure 12). In Figure 13, the temperatures are relatively lower, because only one strip is energized. The best performance is turned in by pattern E_3, although pattens F_3 and B_3 are not far behind.

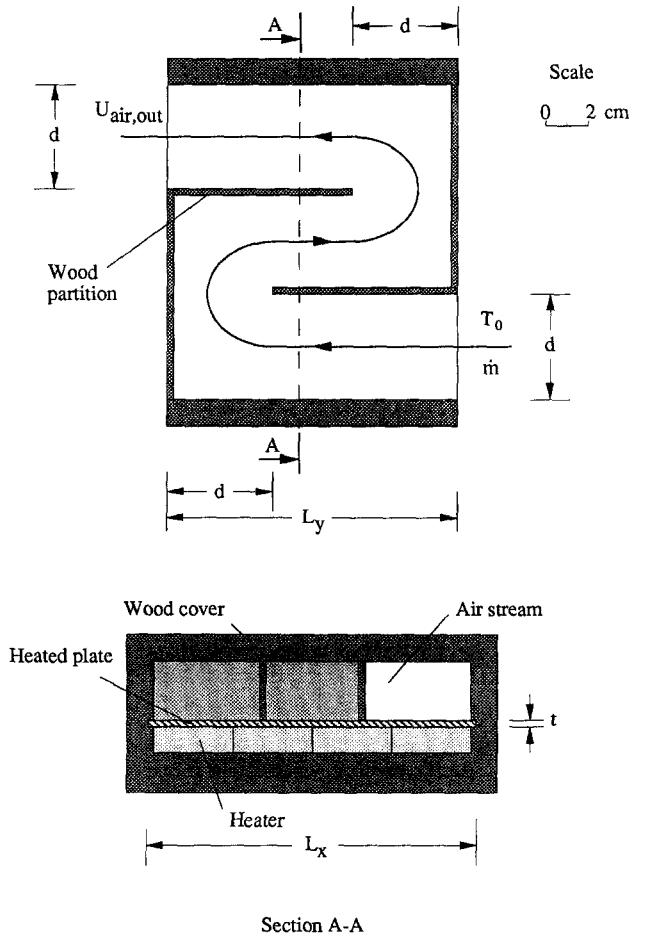

Figure 14 Main features and dimensions of the test section of the experimental apparatus (flow pattern: A_3)

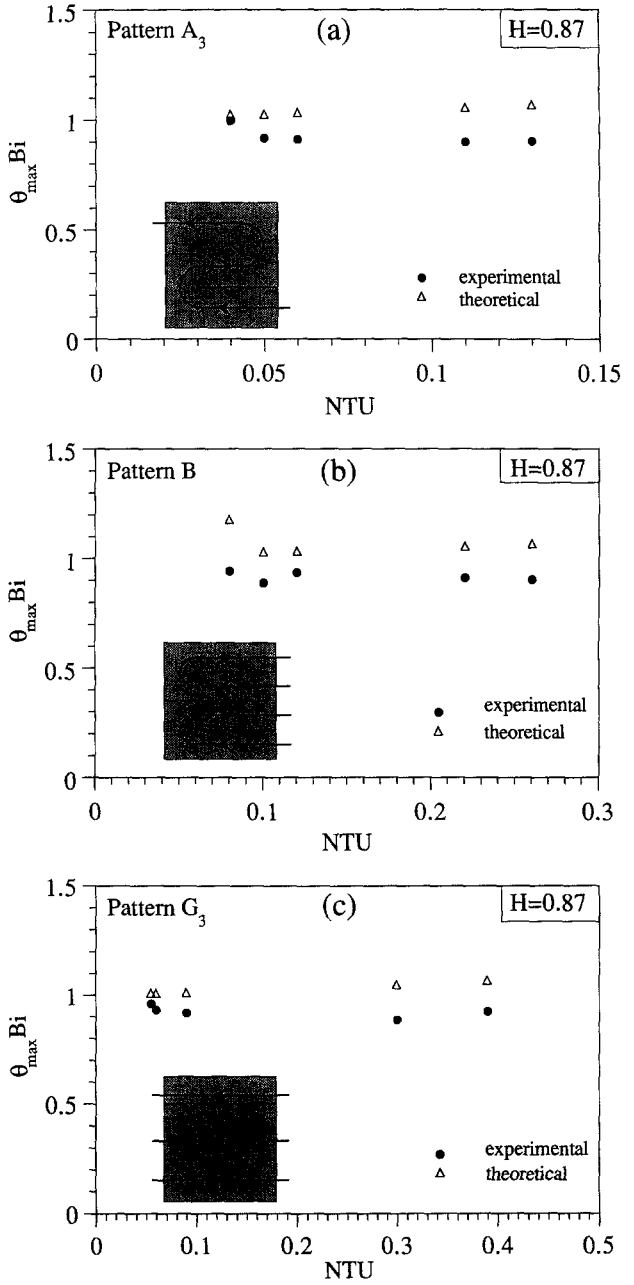

Figure 15 Comparison between the maximum temperatures determined experimentally and theoretically for three flow patterns

Experiments

To illustrate the physical aspects of the analytical and numerical method, we conducted a series of experiments to measure the maximum and minimum temperatures on a rectangular steel plate with a thickness of 3 mm, and $L_x = 159$ mm and $L_y = 138$ mm. The experimental apparatus is shown in Figure 14. The air stream was channelled over the steel plate by using a set of thin wood partitions. Three flow patterns were tested: pattern B of Figure 1a, with a hydraulic diameter D_h of 2.9 cm, and patterns A_3 and G_3 of Figure 12 with $D_h = 3.2$ cm. Heat losses to the room air were minimized by using a 1.75-cm thick wood cover around the test section.

The heaters were connected in parallel and powered by a variable autotransformer that produced voltage between 0 and 140 V. Each heater consisted of a nickel chromium resistance wire strung through and supported by a ceramic core. Finely meshed refractory material fills the remaining air voids to provide good thermal conductivity. The outer cover was seamless stainless steel. Ten copper–constantan-type T thermocouples referenced to an ice-water mixture, were placed in 0.8-mm deep channels machined into the plate. The uncertainty in temperature

Table 2 The dimensionless coordinates (x, y, Figure 1b) of the thermocouple positions

Thermocouple No.	1	2	3	4	5	6	7	8	9	10
x	0.14	0.14	0.26	0.38	0.38	0.62	0.62	0.74	0.86	0.86
y	0.10	0.44	0.77	0.44	0.10	0.10	0.44	0.77	0.44	0.10

Table 3 Measured maximum and minimum temperatures

	θ_{max}			$(\theta_{max}-\theta_{min})/\theta_{max}$		
Re_{in}	Pattern A_3	Pattern B	Pattern G_3	Pattern A_3	Pattern B	Pattern G_3
3750	0.289	0.244	0.261	0.069	0.061	0.115
4750	0.275	0.235	0.241	0.076	0.068	0.124
14100	0.194	0.163	0.177	0.098	0.074	0.147
17900	0.176	0.139	0.157	0.131	0.094	0.159
29200	0.141	0.104	0.119	0.177	0.125	0.185

measurements is 0.84%, resulting from the calibration of the thermocouples.

The apparatus of Figure 14 was installed in the middle of the test section of a suction-type wind tunnel. The test section was a 0.9-m long channel with cross section of 13 cm (width) × 13 cm (height). The air outlet velocity was measured using a calibrated Taylor anemometer. The uncertainty in air velocity is 0.58%. The radiation contributions to the total heat transfer rate was estimated to be less than 1.9%. This insignificant level is attributable to the moderate temperature of the plate: the highest temperature reading was 54.6°C, and the lowest air temperature was 21°C.

We started each run by setting the voltage and current for the resistance heaters and the air stream velocity. We then waited from two to four hours while monitoring the changes in voltage, current, and plate temperatures. We took final readings when the relative changes in voltage, current, and temperature were less than, respectively, 0.2%, 0.2%, and 0.06%. These relative changes were estimated by repeating the run for pattern A_3 at the same Re_{in} value, letting the run last 10 hours. The inlet Reynolds number is $Re_{in} = UD_h/n\nu$ where n is the number of streams.

The calculation of the maximum and minimum temperatures shown in Table 3 was based on measuring the maximum and minimum temperatures and the power dissipated in all the heaters. The error analysis was based on the method of Kline and McClintock (1953). The estimated uncertainty in θ was less than 4%. The uncertainty in Re_{in} is between 10 and 18%. These estimates are also based on the following uncertainties: 0.5% in voltage and 1% in current, 2% in air viscosity, and 2% in steel thermal conductivity (Thermodynamic Properties of Matter 1970).

To estimate the order of magnitudes of Bi, we used Equation 1 in conjunction with the following approximations,

$$\frac{\partial^2\theta}{\partial x^2} \approx 0. \tag{39}$$

$$\frac{\partial^2\theta}{\partial y^2} \approx \frac{1}{y_3-y_1}\left[\frac{\theta(y_3)-\theta(y_2)}{y_3-y_2} - \frac{\theta(y_2)-\theta(y_1)}{y_2-y_1}\right]. \tag{40}$$

$$\theta_c^{(1)}(y_2) \approx \theta_0. \tag{41}$$

where y_1, y_2, and y_3 are the coordinates of the first three thermocouples downstream from the air inlet. The corresponding NTU was calculated from the definition $NTU = Bikt/(\dot{m}c_p)$, where t is the plate thickness. Obtained in this way, Bi and NTU are *inlet* approximations.

To estimate the error in Bi attributable to assuming Equation 39, we considered the worst case where

$$\frac{\partial^2\theta}{\partial x^2} = \frac{\partial^2\theta}{\partial y^2}. \tag{42}$$

This is conservative, because in reality $\partial^2\theta/\partial x^2 < \partial^2\theta/\partial y^2$, because the coolant flows mainly in the y direction. By using Bi and the plate temperatures determined experimentally, we made a new estimate of the Biot number, $Bi_* = 2\,Bi - \theta_{max}/\theta_{min}^2$. In this way, we found that the upper bound of the relative error $|(Bi_* - Bi)/Bi_*|$ was between 0.18 and 0.39 in all the runs documented in Table 4.

Table 4 Comparison between the experimental results (exp) and theoretical results (th) for the maximum temperature

Pattern	Bi	NTU	$(\theta_{max}Bi)_{th}$	$(\theta_{max}Bi)_{exp}$	$1-\frac{(\theta_{max}Bi)_{exp}}{(\theta_{max}Bi)_{th}}$
A_3	3.11	0.11	1.057	0.899	0.149
	3.28	0.13	1.069	0.902	0.156
	4.70	0.06	1.034	0.912	0.118
	5.21	0.05	1.026	0.917	0.106
	7.07	0.04	1.025	0.997	0.027
B	3.70	0.26	1.066	0.903	0.153
	3.88	0.22	1.055	0.912	0.136
	5.74	0.12	1.033	0.936	0.094
	6.39	0.10	1.029	0.888	0.137
	9.06	0.08	1.178	0.942	0.200
G_3	3.55	0.39	1.069	0.927	0.133
	3.69	0.30	1.052	0.889	0.155
	5.20	0.09	1.014	0.920	0.093
	5.94	0.06	1.010	0.933	0.076
	8.09	0.05	1.011	0.963	0.047

Table 4 shows the θ_{max}, Bi, and NTU values for the 15 cases investigated experimentally. The same table also shows the results obtained with the method of the Mathematical formulation through the Numerical results sections for the same flow pattern and (Bi, NTU) pair, which is based on the assumption that Bi is constant along the flow path. This comparison is also illustrated in Figure 15. The average relative difference between the two sets of results is 12%.

Conclusion

In this paper, we showed theoretically and experimentally how the choice of flow pattern influences the temperature distribution in a 2-D conducting space. Special emphasis was placed on ways of reducing the maximum temperature and increasing the temperature uniformity. The cooling patterns consisted of one or more streams making one or more passes.

Future studies may extend the present method in several directions. Rows of concentrated heat sources may be modeled as intermittent strips with heat generation, as illustrated in Figure 13. The method can also be extended to a space with a local (rectangular) heat source inside a larger conducting space, as in Lall et al. (1994). In this case, the analytical formulation will take into account the spectral decomposition of the heat generation intensity function, which will modify the system of differential equations for determining the coolant temperature. By superposition, the method can be generalized to simulate spaces with more than one rectangular heat source inside the space $\mathscr{D}$. Similarly, the method can be generalized (and made more intensive numerically) to account for anisotropic heat conduction, temperature-dependent thermal conductivity, and a heat transfer coefficient that varies along the stream path. An interesting question that is worth examining experimentally is how the flow behaves in the end-turn regions, especially at transitional Reynolds numbers.

The study was conducted in two parts. In the first, we developed an analytical and numerical method for the selection of the flow pattern. In the second part, we showed that the numerical results agree well with measurements. The experimental phase also showed that in the laboratory, the selection of the flow pattern would have do be done by repeatedly building a channel and testing it. The analytical-numerical alternative is considerably faster and less expensive.

Acknowledgment

This work was sponsored by Duke University, the IBM Corporation, Research Triangle Park, NC, and by a grant from the North Carolina Supercomputing Center.

References

Beloff, P. S., Bejan, A. and Campo, A. 1988. Transient natural convection heat transfer in a large-diameter cylinder. *Exp. Thermal Fluid Sci.*, **1**, 267–274

Creel, K. E. and Nelson, D. J. 1994. Criteria for approximating a layer in three-dimensional thermal models of multilayer electronics. *Proc. Intersociety Conference on Thermal Phenomena in Electronics Systems, I-THERM IV*, Washington, DC, 207–213

Deaver, F. K. and Eckert, E. R. G. 1970. An interferometric investigation of convective heat transfer in a horizontal fluid cylinder with wall temperature increasing at a uniform rate. *Proc. 4th Int. Heat Transfer Conference*, Paper NC 1.1

Hingorani, S., Fahrner, C. J., Mackowski, D. W., Goodling, J. S. and Jaeger, R. C. 1994. Optimal sizing of planar thermal spreaders. *J. Heat Transfer*, **116**, 296–301

Kamath, V. 1994. Air injection and convection cooling of multi-chip modules: A computational study. *Proc. Intersociety Conference on Thermal Phenomena in Electronic Systems, I-THERM IV*, Washington, DC, 83–90

Kline, S. J. and McClintock, F. A. 1953. Describing uncertainties in a single-sample experiment. *Mech.. Eng.*

Lall, B. S., Ortega, A. and Kabir, H. 1994. Thermal design rules for electronic components on conducting boards in passively coooled enclosures. *Proc. Intersociety Conference on Thermal Phenomena in Electronic Systems, I-THERM IV*, Washington, DC, 50–61

Moffat, R. J. and Ortega, A. 1988. Direct air cooling of electronic components. In *Advances in Thermal Modeling of Electronic Components and Systems*, Vol. I, A. Bar-Cohen and A. D. Kraus (eds.), Hemisphere, Bristol, PA, 129–282

Peterson, G. P. and Ortega, A. 1990. Thermal control of electronic equipment and devices. *Adv. Heat Transfer*, **20**, 181–314

Sugavanam, R., Ortega, A. and Choi, C. Y. 1994. A numerical investigation of conjugate heat transfer from a flush heat source on a conductive board in laminar channel flow. *Proc. Intersociety Conference on Thermal Phenomena in Electronic Systems, I-THERM IV*, Washington, DC, 62–72

Thermophysical Properties of Matter. 1970. TPRC Data Series, Vols. 1 and 6, Purdue Research Foundation, New York